CHAPTER 3

Effect of Heat Treatment on Electrical and Optical Characteristics of ZnO QDs/MoO_X/Ag Based Photodetectors*

Contents

*Part of this work has been published as:

Hemant Kumar et al. Electrical and Optical Characteristics of Solution processed MoO_x and ZnO QDs Heterojunction. *MRS Communications*, 7(3), 607-612, 2017.

CHAPTER 3

Effect of Heat Treatment on Electrical and Optical Characteristics of ZnO QDs/MoO_X/Ag Based Photodetectors

3.1 Introduction

It has been already discussed in Chapter-1 that the roles of charge transport layers are very important for determining the performance parameters of photodetectors (PDs) (Pal *et al.*, 2012; Baeg *et al.*, 2013) and solar cells (Litzov and Brabec, 2013; Lattante, 2014). Among multiple materials such as ZnO (Pal *et al.*, 2012), TiO_2 (Pal *et al.*, 2012), Cs_2CO_3 (Liao *et al.*, 2008), and Nb_2O_5 (Wiranwetchayan *et al.*, 2011), we have already presented the use of annealed colloidal ZnO QDs based ETL in Chapter-1. For the hole transport layer (HTL) in the PDs, the commonly used materials are PEDOT:PSS (Ionescu-Zanetti *et al.*, 2004; M. Kemerink, S. Timpanaro, M. M. de Kok, E. A. Meulenkamp, 2004), MoO_x (Girotto *et al.*, 2011), NiO (Caruge *et al.*, 2006), WO_3 (M. Kemerink, S. Timpanaro, M. M. de Kok, E. A. Meulenkamp, 2004), and V_2O_5 (Zilberberg *et al.*, 2011). However, for the colloidal QDs based PDs, MoO_x is the most preferred material for the HTL (Litzov and Brabec, 2013; Lattante, 2014) due to its greater air stability to the fabricated device structure over other HTL materials (Chambon *et al.*, 2012). Although MoO_x thin film is normally grown by thermal evaporation (Lattante, 2014), Girotto et al. (Girotto *et al.*, 2011) have observed that the performance of solution processed MoO_3 HTL is nearly same to the thermally deposited MoO_3 HTL for solar cell applications. In view of the above, we will investigate the electrical and optical properties of MoO_x/ZnO QDs based photodetectors for both the thermally grown and solution-processed MoO_x HTL. The effect of post-fabrication heat

treatment at 280°C of the device on the electrical and optical properties of the PDs have also been analyzed for the thermally grown and solution-processed MoO_x HTL on the colloidal ZnO QDs thin film of the device. The layout of this Chapter is given below:

Section 3.2 discusses the experimental techniques used for device fabrication. Section 3.3 provides the analysis of the comparative results between the PDs with thermally grown and solution-processed MoO_x thin film based HTL. Finally, Section 3.4 concludes the major observations of this Chapter.

3.2 Experimental Details

The fabrication of device starts from depositing the ZnO QDs thin film on ITO-coated glass substrates cleaned thoroughly by using alcanox, deionized (DI) water, acetone, and isopropanol subsequently and then dried at 90°C for 15 minutes as discussed in chapter 2. The ZnO QD thin film is deposited over the ITO coated substrate using spin coating technique and then annealed at 250ºC as concluded in chapter 2. The synthesis of MoO_x solution and fabrication of MoO_x/ZnO QDs based photodetectors for thermally grown and solution-processed MoO_x are described in following steps.

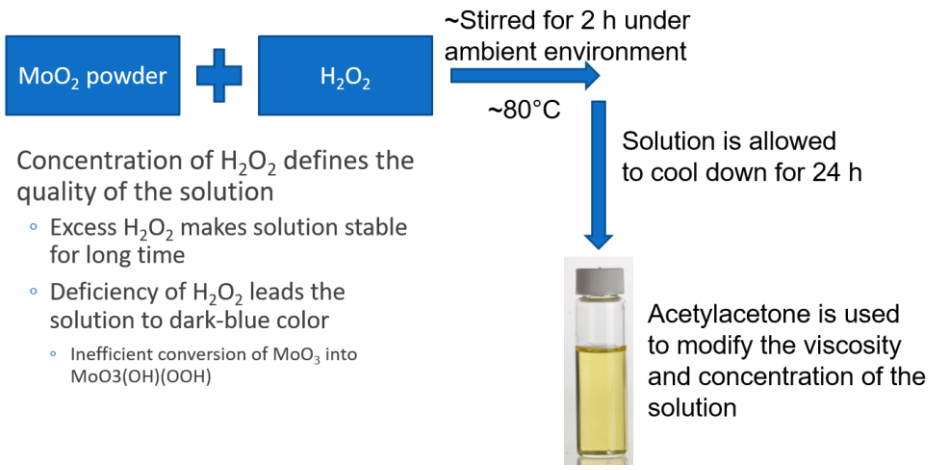

Figure 3.1: Procedure for preparation of MoO_x solution for solution processing deposition.

3.2.1 Preparation of MoO_x Solution

MoO_x solution is prepared using the technique specified by Girroto *et al.* (Girotto *et al.*, 2011) details shown in Figure 3.1. 1 M solution of MoO_2 powder is stirred with H_2O_2 for ~2 h at 80°C under the ambient environment and then allowed to cool down for 24 h to obtain a clear yellow liquid. Acetylacetone is further used to modify the viscosity and concentration of the solution. The concentration of H_2O_2 defines the quality of the solution; excess H_2O_2 makes the solution stable for a long duration while it changes to dark-blue solution due to the insufficient conversion of MoO_3 into MoO_3(OH)(OOH) under the deficiency of H_2O_2 (Girotto *et al.*, 2011).

3.2.2 Device Fabrication

For preparing the MoO_x/ZnO QDs heterojunction by solution processed method, the prepared solution of MoO_x described earlier is spin-coated on ITO/ZnO QDs substrate. The solution deposited MoO_x is annealed at 270°C for crystallization and removal of organic solvents. The process is repeated to achieve a 30-35 nm thickness of the MoO_x measured by using Reflectometer (F-20 Thin Film UV Analyzer, Filmetrics). For fabricating the second type of device, MoO_x is deposited on the ITO/ZnO QDs by a thermal evaporation method to achieve a thickness of ~30 nm. Thermal evaporation (HHV, FL400 SMART COAT 3.0) is also used for the deposition of high purity Ag (99.99%) of ~ 50 nm thickness on both the solution processed and thermally deposited MoO_x HTL layer. Thermal deposition of both the materials (MoO_x and Ag) was performed at a vacuum of ~10^{-6} bar and at variable deposition rates (for first 5 nm thickness: 0.1 Å/s; for 5 – 20 nm thickness: 0.5 Å/s, and for above 20 nm thickness: 1 Å/s). The thickness of the deposited thin films and the rate of evaporation are monitored using digital thickness monitor (INFICON model no. SQM-160) attached to the coating

unit. The two types of Ag/MoO_x/ZnO QDs/ITO based complete heterojunction devices are annealed under ambient environment for 30 mins at 280°C. The schematic of the device under study for MoO_x grown by solution processing and thermal evaporation are shown in Figure 3.2.

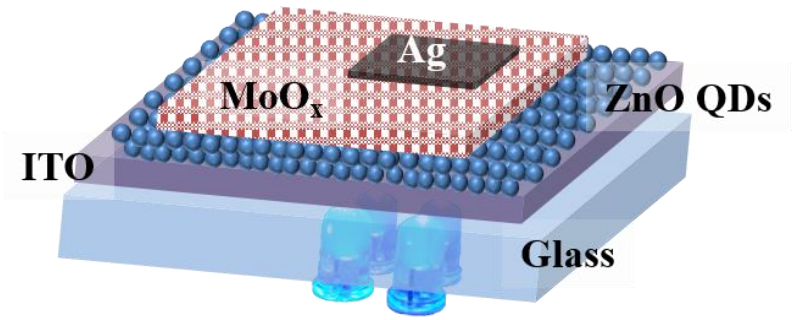

Figure 3.2: Complete schematic device structure of the solution-processed and thermally grown MoO_x.

3.3 Results and Discussion

3.3.1 Structural Characterization

The high-resolution scanning electron microscopy (HRSEM: SUPRA 40, Zeiss) image of the complete device structure with solution processed and thermally grown MoO_x is performed before and after the heat treatment of the complete devices as shown in Figure 3.3. The HRSEM of solution processed MoO_x based diode shows the stability of the device as the layers are distinguished after the heat treatment and indicate separable interface between MoO_x and ZnO QDs as shown in Figure 3.3 (a) and (b). Similarly, HRSEM of the diode with thermally evaporated MoO_x is performed and shown in Figure 3.3 (c) and (d). The device after heat treatment shows the continuous interface between thermally grown MoO_x and ZnO QDs which may be due to the diffusion of MoO_x into the ZnO QDs shown in Figure 3.3 (d). Furthermore, the annealing of the thin films greatly improves the morphology and interface characteristics of the devices and materials. Thermally deposited MoO_x does not show

any grains in Figure 3.3 (c), but after the heat treatment of the complete device the grain boundaries are visible leading to the crystallization of the MoO_x thin film shown in Figure 3.3 (d).

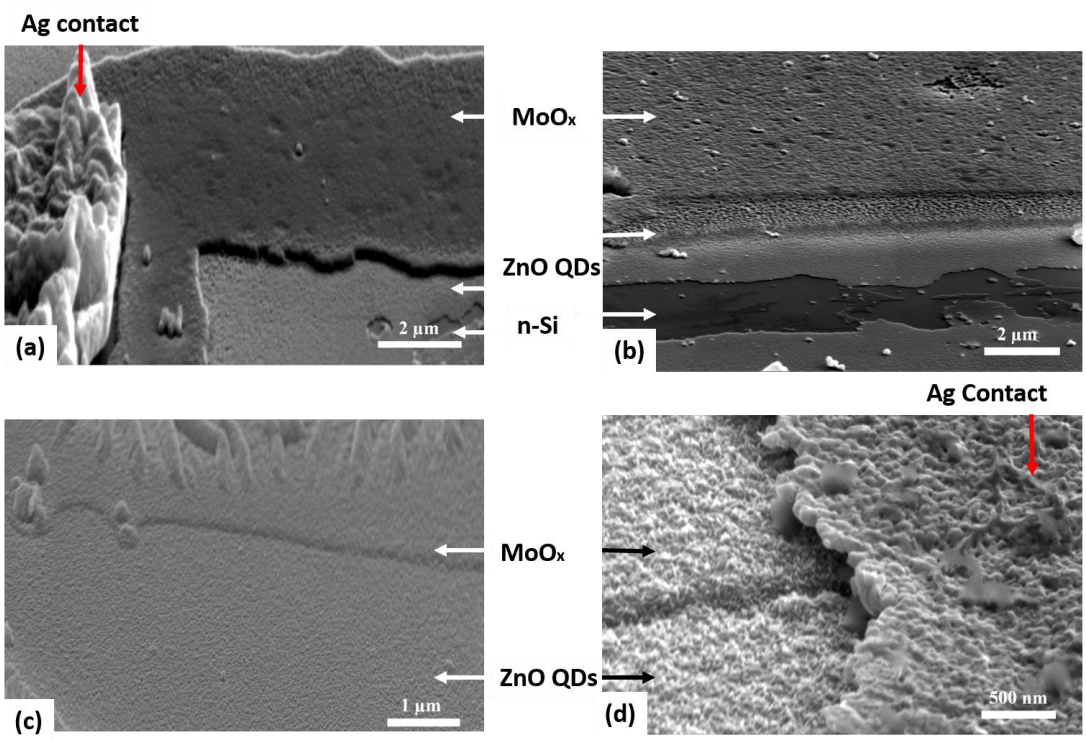

Figure 3.3: HRSEM image of (a) solution-processed MoO_x-based device before annealing at 280°C, (b) solution-processed MoO_x-based device after annealing at 280°C, (c) thermally grown MoOx-based device before annealing at 280°C, and (d) thermally grown MoO_x-based device after annealing at 280°C.

3.3.2 Optical Characterization

The study of optical properties of MoO_x and ZnO QDs are analyzed in this section. The photoluminescence emission (PL) and excitation (PLE) spectrum of ZnO QDs and MoO_x are shown in Figure 3.4 (a) and (b), respectively. The PLE spectrum of ZnO QDs shows a peak at 365 nm (3.39 eV), the curve of absorption spectra is fitted to match the wavelength axis. The peak of PLE spectrum for MoO_x is obtained at ~400 nm, and the same is also shown in Figure 3.4 (a) and (b). The PL spectrum of the material provides

great details about the monodispersity of the nanocrystals, quality of the film or synthesized material, and interface defects if any.

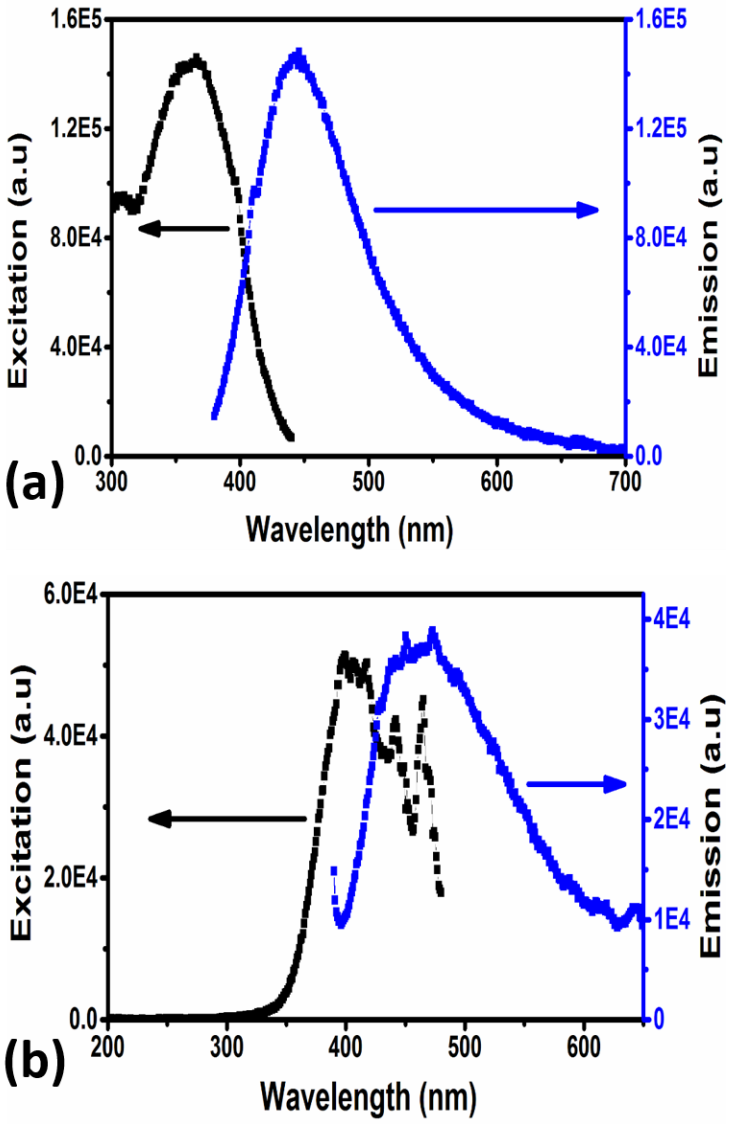

Figure 3.4: (a) Photoluminescence (PL) excitation and emission spectrum of colloidal ZnO QDs solution and (b) PL excitation and emission spectrum of MoO_x-solution.

The PL spectrum of ZnO QDs shown in Figure 3.4 (a) shows the narrow-band emission spectrum with a full width at half maximum (FWHM) of 72 nm. The selectivity of ZnO QDs PL indicates the high-quality and monodispersity of the ZnO QDs. The PL spectrum of MoO_x shown in Figure 3.4 (b) have the FWHM of 125 nm

and shows no trailing edges indicates that the MoO_x are free from any surface defects. The involvement of surface defects increases the charge trapping sites.

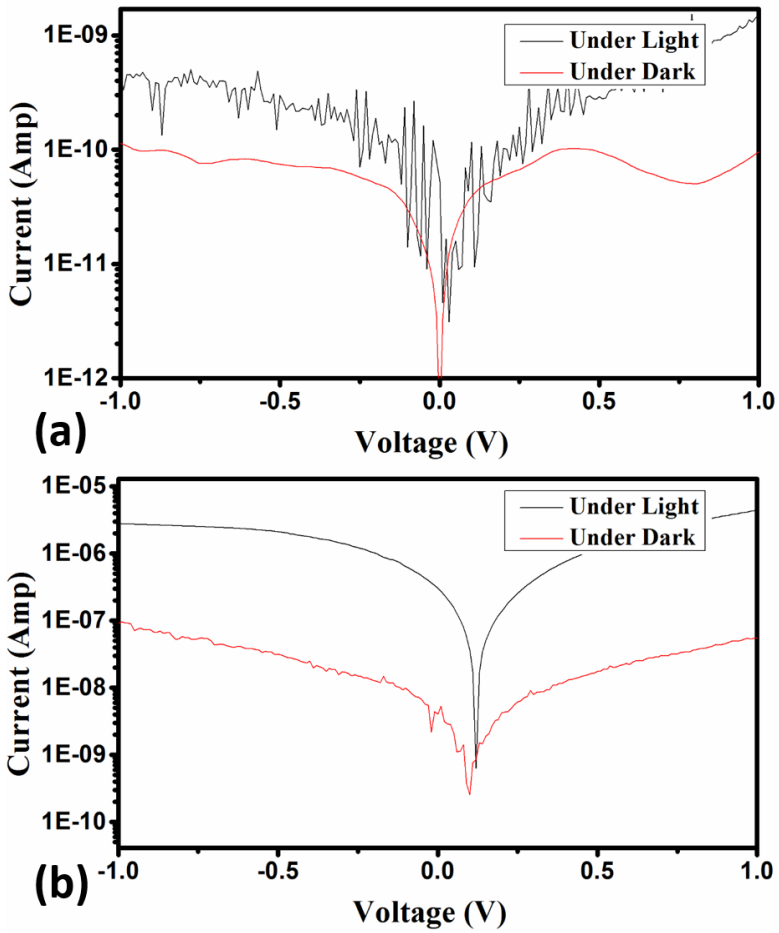

Figure 3.5: Logarithmic current-voltage curve under light and dark condition for (a) solution-processed MoO_x-based diode without annealing and (b) solution-processed MoO_x-based diode after annealing.

3.3.3 Electrical Characterization

The current versus voltage (I-V) relationship for the devices with MoO_x grown by solution processing and thermal evaporation are shown in Figure 3.5 and Figure 3.6, respectively, measured using Keysight B1500A from -1 V to +1 V. The I-V curve is plotted under the dark and under the illumination of UV light (UV LED source with an optical power density of 800 µW/cm^2 at 365 nm). The effect of heat treatment on the

complete device is evident in both devices as the dark current (noise current) increases with the annealing.

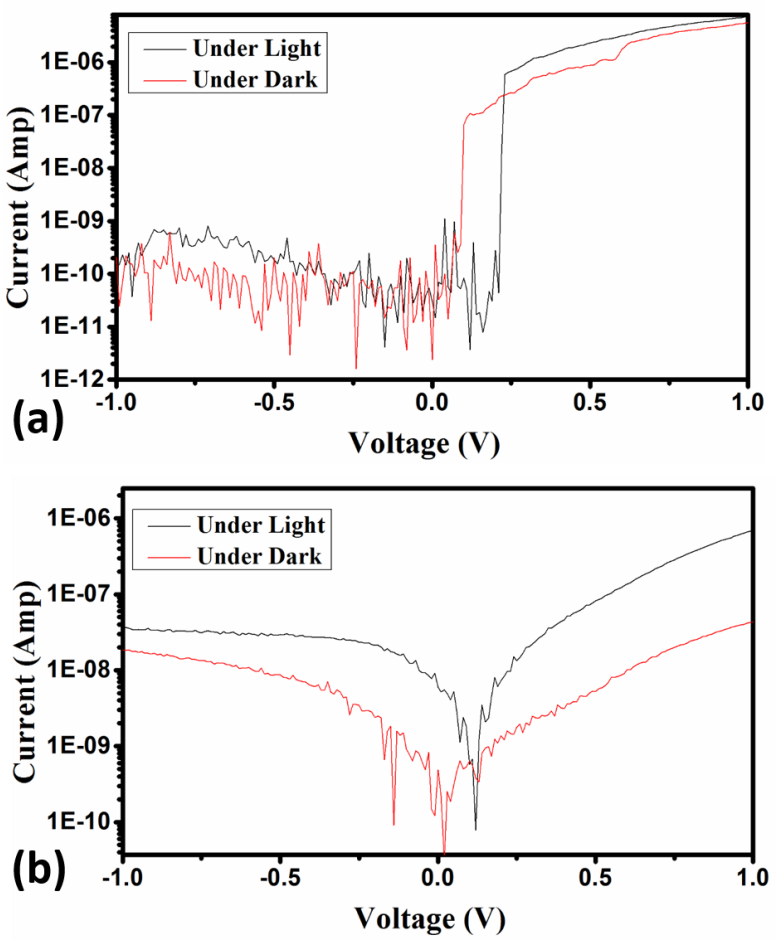

Figure 3.6: Logarithmic current-voltage curve under light and dark condition for (a) thermally grown MoO_x-based diode without annealing and (b) thermally grown MoO_x-based diode with annealing.

The solution-processed MoO_x based device shows superior photoresponse after heat treatment compared to the device without heat treatment. Furthermore, the stability of the photocurrent is also observed in Figure 3.5 (b) compared to Figure 3.5 (a) and the contrast ratio (I_{ph}/I_{dark}) of the device enhanced from 3.88 to 38.72 at an applied bias of -1 V. The thermally grown MoO_x based device shows deterioration in rectifying nature of the device and the noise current is increased by ratio of greater than ~100 times shown in Figure 3.6 (a) and (b). This deterioration of the device is due to the diffusion

of MoO_x into the ZnO QDs which varies the barrier between the ZnO QDs and MoO_x from graded to the linear junction. The photoresponse of the devices can be compared using the responsivity of the device calculated using Equation 2.5. The measured responsivity of the devices with and without heat treatment under the illumination of UV LED at an applied bias of -1 V are indicated in Table 3.1. The slight shift of zero current in Figure 3.5 and Figure 3.6 may be attributed to the increased size of ZnO QDs with improved crystinality and modified interfaces between two QDs due to the annealing of the films.

Table 3.1: Responsivity of the fabricated devices under the optical power density of 800 μW/cm^2 at 365 nm.

Devices	**Solution-processed MoO_x based device**		**Thermally deposited MoO_x based device**	
	Before heat treatment	**After heat treatment**	**Before heat treatment**	**After heat treatment**
Responsivity (A/W)	5.46×10^{-7}	3.93×10^{-3}	1.82×10^{-7}	5.72×10^{-5}
Contrast Ratio	3.88	38.72	1.41	1.61

The A^2/C^2 versus voltage curve for solution processed and thermally grown MoO_x based device after heat treatment is shown in Figure 3.7. The heterojunction between MoO_x and ZnO QDs is assumed to be a Schottky junction, and therefore most of the depletion region will reside in ZnO QDs thin film. The curves are shown in Figure 3.7 can be interpreted as (Sze, 2002):

$$\frac{A^2}{C^2} = \frac{2}{q\varepsilon}\left(\frac{\phi - V}{N_d}\right) \tag{3.1}$$

where N_d is the donor concentration in n-type layer, ε is the effective dielectric

constant of the ZnO QDs film, q is the electron charge, and ϕ is built-in potential. From the projected intersection of capacitance curve in voltage axis we find the value of built-in potential and found to be 0.25 V and 0.046 V for solution processed and thermally grown MoO_x based device, respectively. Thus, the low built-in potential shown by a diode (for thermally grown MoO_x) indicates the junction between ZnO QDs and MoO_x is not abrupt but the linear in nature. The ideality factor of the diodes are also calculated and found to be 3.85 and 6.14 for solution processed and thermally grown MoO_x based device, respectively.

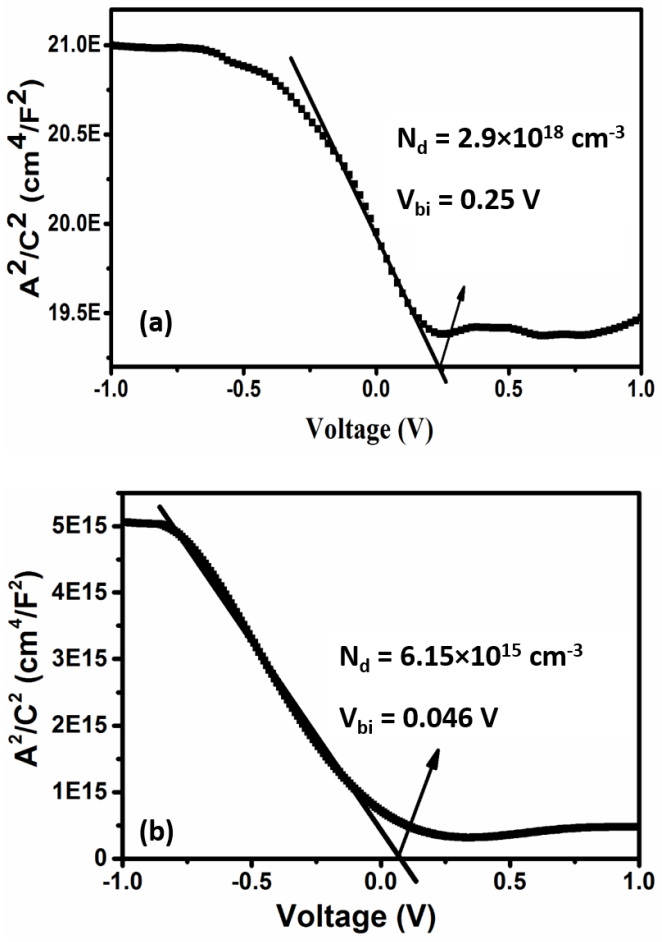

Figure 3.7: A^2/C^2 versus voltage curve for (a) solution-processed MoO_x-based diode and (b) thermally processed MoO_x-based diode.

The ideality factor defines the quality of the diode (junction). Ideally, the value of ideality factor should be equal to 1, but due to interface defects this result deviates from 1 and tends to increase >1. The high value of ideality factor 6.14 also indicates the low quality of junction formed between thermally grown MoO_x and ZnO QDs.

3.4 Conclusion

In this chapter, the electrical and optical properties of the solution processed and thermally grown MoO_x HTL based Ag/MoO_x/ZnO QDs heterojunction PDs with and without post-device fabrication annealing have been investigated possibly for the first time. The solution processed and thermally grown MoO_x based devices are heat treated (post-device fabrication) at 280^{o}C under the ambient condition for 30 mins. The responsivity of the solution-processed MoO_x based PD after heat treatment is 3.93 mA/W at 365 nm which is ~7198 times higher than solution processed MoO_x without heat treatment. On the other hand, the thermally grown MoO_x HTL based heterojunction PD shows the responsivity of 1.82×10^{-7} and 5.72×10^{-5} before and after the post-fabrication heat treatment. After annealing, the built-in potential and ideality factor for the solution processed MoO_x based heterojunction are 0.25 V and 3.85 whereas the built-in potential and ideality factor for the thermally grown MoO_x based heterojunction is 0.046 V and 6.14 respectively. Thermally grown MoO_x based device also shows an increase in the noise current of about 100 times after heat treatment of the device. In brief, the solution processed MoO_x HTL provide better device stability compared to the thermally grown MoO_x HTL at an expense of higher annealing temperature at 270^{o}C in the fabrication of the colloidal QDs based photodetectors